

NASA TN D-5071

**NASA TECHNICAL NOTE**



**NASA TN D-5071**

C.1



TECH LIBRARY KAFB, NM

LOAN COPY: RETURN TO  
AFWL (WLIL-2)  
KIRTLAND AFB, N MEX

**EXPERIMENTAL VERIFICATION OF  
SCALE FACTORS FOR PARAWING OPENING  
CHARACTERISTICS WITH DIMENSIONAL  
RATIOS FROM 1:1.3 TO 1:3**

*by Robert H. Moore, David L. Eichblatt,  
and Theodore F. Hughes*

*Manned Spacecraft Center  
Houston, Texas*

NATIONAL AERONAUTICS AND SPACE ADMINISTRATION • WASHINGTON, D. C. • MARCH 1969



0131922

EXPERIMENTAL VERIFICATION OF SCALE FACTORS  
FOR PARAWING OPENING CHARACTERISTICS WITH  
DIMENSIONAL RATIOS FROM 1:1.3 TO 1:3

By Robert H. Moore, David L. Eichblatt,  
and Theodore F. Hughes

Manned Spacecraft Center  
Houston, Texas

NATIONAL AERONAUTICS AND SPACE ADMINISTRATION

---

For sale by the Clearinghouse for Federal Scientific and Technical Information  
Springfield, Virginia 22151 - CFSTI price \$3.00

## ABSTRACT

Verification of an analytical scaling technique by experimental drop tests under controlled conditions is presented in which opening characteristics of full-scale flexible parawing and an intermediate-scale model are predicted from results of model testing. Two methods of scaling are considered, dynamic similarity and wing loading. Dynamic similarity is derived from comparing similar forces in the equation of motion of scale models to those of a prototype. Wing loading is similar but differs by requiring the payload-weight-per-canopy area of all parawings to be the same. Three scaled, all-flexible parawings with keel lengths of 8, 18, and 24 feet were tested at initial opening velocities ranging from 46 to 90 feet per second. Results are presented in the form of comparisons of actual and predicted tension, acceleration, velocity, and distance time histories. Scaling by the dynamic-similarity method predicted the opening characteristics of full-scale parawings within the repeatability of the data, but the wing-loading method was found to be deficient.

## CONTENTS

Section	Page
SUMMARY . . . . .	1
INTRODUCTION . . . . .	1
SYMBOLS . . . . .	2
THEORY . . . . .	4
Dynamic Similarity . . . . .	4
Wing Loading . . . . .	7
PARAWINGS AND TESTING COMPONENTS . . . . .	12
Parawing . . . . .	13
Load-Measuring System . . . . .	14
Payload . . . . .	14
Canopy-Packing Sleeves . . . . .	15
Automatic Release Mechanism . . . . .	15
DEPLOYMENT TEST . . . . .	15
DATA REDUCTION . . . . .	19
RESULTS . . . . .	20
Repeatability . . . . .	20
Small-Scale Model Deployment Characteristics . . . . .	21
Intermediate-Scale Model Deployment Characteristics . . . . .	22
Full-Scale Model Deployment Characteristics . . . . .	24
Averaging Technique . . . . .	24
Dynamic-Similarity Results . . . . .	25
Wing-Loading Results . . . . .	32

Section	Page
CONCLUDING REMARKS . . . . .	33
REFERENCES . . . . .	34

## TABLES

Table	Page
I      SCALE FACTORS USED FOR DYNAMIC SIMILARITY . . . . .	8
II     SCALE FACTORS USED FOR WING LOADING . . . . .	11
III    SYSTEM WEIGHTS AND DIMENSIONS . . . . .	15
IV    TENSION CORRECTION FACTOR . . . . .	20

## FIGURES

Figure		Page
1	Parawing canopy planform . . . . .	13
2	General parawing payload with testing equipment . . . . .	14
3	Parawing folding technique . . . . .	16
4	Parawing packing technique . . . . .	16
5	Parawing positioned for deployment . . . . .	17
6	Deployment sequence of intermediate model parawing . . . . .	18
7	Small-scale model deployment characteristics	
	(a) Low velocity, 46.3 fps . . . . .	21
	(b) Medium velocity, 51.8 fps . . . . .	21
	(c) High velocity, 56.7 fps . . . . .	22
8	Intermediate-scale model deployment characteristics	
	(a) Low velocity, 69.5 fps . . . . .	23
	(b) Medium velocity, 77.7 fps . . . . .	23
	(c) High velocity, 85.1 fps . . . . .	23
9	Full-scale deployment characteristics	
	(a) Low velocity, 80.2 fps . . . . .	24
	(b) Medium velocity, 89.7 fps . . . . .	24
10	Comparison of small-scale predicted and intermediate-scale average tension time histories	
	(a) Low velocity, 69.5 fps . . . . .	25
	(b) Medium velocity, 77.7 fps . . . . .	26
	(c) High velocity, 85.1 fps . . . . .	26
11	Comparison of small-scale predicted and intermediate-scale average acceleration time histories	
	(a) Low velocity, 69.5 fps . . . . .	27
	(b) Medium velocity, 77.7 fps . . . . .	27
	(c) High velocity, 85.1 fps . . . . .	27

Figure		Page
12	Comparison of small-scale predicted and intermediate-scale average velocity time histories	
	(a) Low velocity, 69.5 fps . . . . .	28
	(b) Medium velocity, 77.7 fps . . . . .	28
	(c) High velocity, 85.1 fps . . . . .	28
13	Comparison of small-scale predicted and intermediate-scale average distance time histories	
	(a) Low velocity, 69.5 fps . . . . .	29
	(b) Medium velocity, 77.7 fps . . . . .	29
	(c) High velocity, 85.1 fps . . . . .	29
14	Comparison of small- and intermediate-scale predicted and full-scale average tension time histories	
	(a) Low velocity, 80.2 fps . . . . .	30
	(b) Medium velocity, 89.7 fps . . . . .	30
15	Comparison of small- and intermediate-scale predicted and full-scale average acceleration time histories	
	(a) Low velocity, 80.2 fps . . . . .	30
	(b) Medium velocity, 89.7 fps . . . . .	30
16	Comparison of small- and intermediate-scale predicted and full-scale average velocity time histories	
	(a) Low velocity, 80.2 fps . . . . .	31
	(b) Medium velocity, 89.7 fps . . . . .	31
17	Comparison of small- and intermediate-scale predicted and full-scale average distance time histories	
	(a) Low velocity, 80.2 fps . . . . .	31
	(b) Medium velocity, 89.7 fps . . . . .	31
18	Small-scale deployment characteristics (based on wing loading); velocity = 80.2 fps . . . . .	32
19	Comparison of predicted and average tension time histories (based on wing loading); velocity = 80.2 fps . . . . .	33

**EXPERIMENTAL VERIFICATION OF SCALE FACTORS  
FOR PARAWING OPENING CHARACTERISTICS WITH  
DIMENSIONAL RATIOS FROM 1:1.3 TO 1:3**

By Robert H. Moore, David L. Eichblatt,  
and Theodore F. Hughes\*  
Manned Spacecraft Center

**SUMMARY**

An experimental verification of an analytical scaling technique is presented which predicts the opening characteristics of a lifting-type parachute from results obtained by model testing. Two methods of scaling were considered. One method, dynamic similarity, is derived from comparing like forces in the equations of motion of scale models to those of a prototype; the other method, wing loading, is similar but differs by requiring the payload-weight-per-canopy area of the parawings to be the same.

Three scaled, all-flexible parawings were tested: a scale model having a keel length of 8 feet and a payload of 5 pounds, an intermediate-scale model having a keel length of 18 feet and a payload of 78 pounds, and a full-scale model having a keel length of 24 feet and a payload of 191 pounds. Dimensions and weights were scaled to obtain corresponding dynamic similarity. The parawings were deployed from an initial packed condition and at various initial velocities. Results from the measured opening characteristic tests of the models were scaled according to the techniques to predict the full-scale results. A comparison of predicted results to measured results confirms the value of dynamic similarity of model scaling on deployment characteristics of parawings. Scaling by the wing-loading technique proved to be deficient within the scope of the test program.

**INTRODUCTION**

With the exception of the opening characteristics, results of model testing have been most useful to the early design stages of full-scale parachutes.

Until the concept of dynamic similarity was applied to parachute openings (ref. 1), model opening characteristics were not applicable to full-scale opening characteristics because of the lack of an acceptable scaling method. This technique describes a

---

\* ITT/Federal Electric Corp.

method in which dynamic similarity is obtained by comparing like forces in the equations of motion of conventional parachutes. For further confirmation, reference 2 describes a testing program in which the technique was applied to deployment characteristics of lifting-type parachutes (parawings). The parawings were of physical size ratios of 1:2.

An extension to these programs is presented in this report in which the analytical scaling technique is applied to opening characteristics of larger parawings of physical size ratios of 1:3. In addition, an attempt was made to scale the parawing opening characteristics by forcing the payload-weight-per-canopy area (wing loading) of each parawing to be equal. This method of scaling has significant differences when compared to the method of dynamic similarity. This technique has been the primary method used in the early design stages of parachutes, but has not been successful yet in predicting deployment characteristics of full scales from model information.

Three scaled, all-flexible parawings were tested: a small-scale model having a keel length of 8 feet and a payload of 5 pounds, an intermediate-scale model having a keel length of 18 feet and a payload of 78 pounds, and a full-scale model having a length of 24 feet and a payload of 191 pounds.

The small-scale model was deployed several times each at velocities of 46.3, 51.8, and 56.7 fps while riser tension time histories were recorded. The velocities were obtained at the beginning of canopy extraction. Results obtained were scaled according to the theory of dynamic similarity to predict the intermediate-scale and full-scale results. One series of drops was made at a deployment velocity of 80.2 fps with a payload weight of 25 pounds. The drop results of the later series were scaled by the wing-loading techniques to predict the full-scale results.

Similarly, the intermediate model was deployed at velocities of 69.5, 77.7, and 85.1 fps. The results of the low- and medium-velocity cases were scaled by dynamic similarity to predict the full-scale results.

The full-scale parawing was deployed at velocities of 80.2 and 89.7 fps to provide data for correlation purposes.

#### SYMBOLS

$C_D$  drag coefficient

$C_L$  lift coefficient

CF correction factor

D drag force, lb

d reference length, ft

F force, lb

$g$	gravity, $\text{fps}^2$
$L$	lift force, lb
$m$	mass, slugs
$\dot{m}$	mass flow, slug/sec
$N$	force scale factor
$q$	dynamic pressure, $\text{lb}/\text{ft}^2$
$R$	ratio
$S$	projected area, $\text{ft}^2$
$T$	riser tension, lb
$t$	time, sec
$V$	volume, $\text{ft}^3$
$v$	velocity, fps
$v_\infty$	free stream velocity, fps
$\dot{v}$	acceleration, $\text{fps}^2$
$W$	weight, lb
$WL$	wing loading
$x$	distance, ft
$\gamma$	flight-path angle of attack, degrees
$\rho$	atmospheric density, $\text{slug}/\text{ft}^3$
$\rho_s$	structural density, $\text{slug}/\text{ft}^3$

Subscripts:

f full scale

m model

P.L. payload

All subscripts used with symbol R (ratio) are defined in the basic symbols.

## THEORY

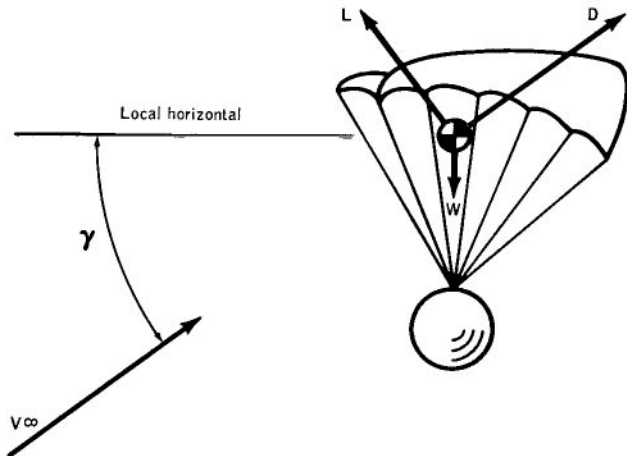
### Dynamic Similarity

To scale the characteristics of parachutes, the equations of motion must be considered. The equations are along the flight path

$$\Sigma F = m\dot{v} + \dot{m}v = D - W \sin \gamma \quad (1)$$

and normal to the flight path

$$\Sigma F = mv\dot{\gamma} = L - W \cos \gamma \quad (2)$$



By the laws of dynamic similarity, as applied to theoretical scaling, all forces in the model equations of motion must be scaled similarly to the same force as the full-scale equations of motion.

$$\frac{(m\dot{v})_m}{(m\dot{v})_f} = \frac{(m\dot{v})_m}{(m\dot{v})_f} = \frac{(mv\dot{\gamma})_m}{(mv\dot{\gamma})_f} = \frac{(W \cos \gamma)_m}{(W \cos \gamma)_f} = \frac{(W \sin \gamma)_m}{(W \sin \gamma)_f} = \frac{(L)_m}{(L)_f} = \frac{(D)_m}{(D)_f} = N \quad (3)$$

or

$$R_{m\dot{v}} = R_{\dot{m}v} = R_{mv\dot{\gamma}} = R_{W\cos\gamma} = R_{W\sin\gamma} = R_L = R_D = N \quad (4)$$

To determine the force scale factor  $N$  in its most basic form, the weight scale factor is expanded to yield

$$R_{W\cos\gamma} = R_m R_g = R_{\rho_s} R_V R_g = R_{\rho_s} R_d^3 R_g = N \quad (5)$$

where use is made of the relations  $W = mg = \rho_s V g$ ,  $V \propto d^3$ , and  $R_{\rho_s} = R_\rho$  (ref. 1).

By referring to the sketch, it can be seen that the flight-path angle can be found in terms of the lift and drag forces.

$$\tan \gamma = \frac{D}{L} \quad (6)$$

From this, the ratio of the tangents becomes

$$R_{\tan\gamma} = \frac{R_D}{R_L} \quad (7)$$

$$R_{\tan\gamma} = \frac{R_{\rho_s} R_g R_d^3}{R_{\rho_s} R_g R_d^3} = 1 \quad (8)$$

and gives rise to the conclusion that the flight-path-angle ratio  $R_\gamma$  must be unity.

Coupled with this information, the weight ratios can be simplified further by the following

$$R_{W\sin\gamma} = \frac{(W \sin \gamma)_m}{(W \sin \gamma)_f} = R_{\rho_s} R_d^3 R_g \quad (9)$$

$$\frac{(W \sin \gamma)_m}{(W \sin \gamma)_f} = \frac{W_m}{W_f} = R_W = R_{\rho_s} R_d^3 R_g \quad (10)$$

where the ratio of the sines is unity. Similarly,  $R_{W\cos\gamma} = R_W$  since the ratio of the cosines also must be unity.

From this point, the derivation of the remaining scale factors remains the same as described in reference 1 with the exception of the scale factors for the lift and drag coefficients. For the lift coefficient, equation (3) yields

$$\left. \begin{aligned} \frac{(qSC_L)_m}{(qSC_L)_f} &= N \\ R_q R_s R_{C_L} &= R_{\rho_s} R_g R_d^3 \end{aligned} \right\} \quad (11)$$

Solving for the ratio of the model to full-scale lift coefficient gives

$$R_{C_L} = \frac{R_{\rho_s} R_g R_d^3}{R_\rho R_v^2 R_d^2} = \frac{R_{\rho_s} R_g R_d^3}{R_\rho R_g R_d R_d^2} = 1 \quad (12)$$

Therefore, the model and full-scale lift coefficients must be equal, and in a similar fashion the drag coefficients must be equal.

$$R_{C_D} = 1 \quad (13)$$

Table I presents the results of the analytical prediction for all factors concerned. The "Test condition" column shown in the table was tabulated because gravity and density ratios were assumed to be equal to 1.0 throughout the program.

#### Wing Loading

Another technique for scaling parachute characteristics is to force the model velocity to equal the velocity of the full scale by matching wing loading.

$$\frac{(W/S)_m}{(W/S)_f} = \frac{R_W}{R_S} = R_{WL} = 1.0 \quad (14)$$

By making this assumption,

$$R_S \propto R_d^2 \quad (15)$$

the weight ratio will become

$$\frac{R_W}{R_S} = 1.0 \quad (16)$$

$$R_W = R_S = R_d^2 \quad (17)$$

where flight-path-angle ratios are unity.

TABLE I. - SCALE FACTORS USED FOR DYNAMIC SIMILARITY

Quantity	Ratio	Result	Test condition
Diameter	$R_d$	$R_d$	$R_d$
Area	$R_s$	$R_d^2$	$R_d^2$
Volume	$R_V$	$R_d^3$	$R_d^3$
Gravity	$R_g$	$R_g$	1.0
Density	$R_\rho$	$R_\rho$	1.0
Distance	$R_x$	$R_d$	$R_d$
Velocity	$R_v$	$R_g^{1/2} R_d^{1/2}$	$R_d^{1/2}$
Acceleration	$R_{\dot{v}}$	$R_g$	1.0
Time	$R_t$	$R_g^{-1/2} R_d^{1/2}$	$R_d^{1/2}$
Mass	$R_m$	$R_\rho R_d^3$	$R_d^3$
Mass flow	$R_{\dot{m}}$	$R_\rho R_g^{1/2} R_d^{5/2}$	$R_d^{5/2}$
Weight	$R_w$	$R_\rho R_g R_d^3$	$R_d^3$
Drag coefficient	$R_{C_D}$	1.0	1.0
Lift coefficient	$R_{C_L}$	1.0	1.0
Flight-path angle	$R_\gamma$	1.0	1.0
Angular velocity	$R_{\dot{\gamma}}$	$R_g^{1/2} R_d^{-1/2}$	$R_d^{-1/2}$

With this basic ground rule laid, the assumption that  $R_{\rho_s} = 1.0$  is no longer valid (eq. (5)).

$$R_W = N = R_{\rho_s} R_g R_d^3 \quad (18)$$

$$R_W = R_d^2 = R_{\rho_s} R_g R_d^3 \quad (19)$$

Solving for  $R_{\rho_s}$  gives

$$R_{\rho_s} = R_d^{-1} \quad (20)$$

where, for earth application,  $R_g = 1.0$ .

Also,  $R_{\rho} = 1.0$  still holds as long as model testing and full-scale testing are conducted in the same atmospheric conditions.

Further proof of  $R_{\rho_s} = R_d^{-1}$  is given by considering the mass ratio which is

$$R_m = \frac{R_W}{R_g} = R_d^2 \quad (21)$$

$$R_m = R_{\rho_s} R_V = R_d^2 \quad (22)$$

where  $R_V \propto R_d^3$

$$R_{\rho_s} = \frac{R_d^2}{R_V} = \frac{1}{R_d} \quad (23)$$

Solving for the acceleration scale factor yields

$$R_m R_{\dot{v}} = R_{\rho_s} R_V R_{\dot{v}} = N \quad (24)$$

$$R_{\dot{v}} = \frac{R_{\rho_s} R_g R_d}{R_{\rho_s}^2 R_d^3} \quad (25)$$

$$R_{\dot{v}} = 1 \quad (26)$$

Similarly, the velocity scale factor is derived from the drag-force scale factor

$$R_D = R_{\rho} R_v^2 R_s R_{C_D} = N = R_{\rho_s} R_g R_d^3 \quad (27)$$

$$R_v^2 = \frac{R_{\rho_s} R_g R_d}{R_{\rho} R_d^2 R_{C_D}} \quad (28)$$

$$R_v = 1.0 \quad (29)$$

where  $R_{C_D}$  is assumed to be unity.

From these relations, it can easily be seen that the time scale factor is

$$R_t = \frac{R_v}{R_{\dot{v}}} = 1.0 \quad (30)$$

and the distance scale factor becomes

$$R_x = R_v R_t = 1.0 \quad (31)$$

Upon comparing the two methods of scaling, it is noticeable that they appear very similar since both are derived from the same equation. The wing-loading restriction simplifies the scale factors as more factors become equal to one, but two fundamental problems arise from the wing-loading restrictions.

First, mass analytically scales as a function of the reference length squared. No problem arises from the payload and structural masses as their values may be scaled correctly by proper selection of materials; but apparent mass is a function of the parachute canopy volume, which scales as the reference length cubed. The apparent mass then will be scaled incorrectly by wing loading. Secondly, the model must translate the same distance as the full-scale system and yet have altogether different scaled lengths.

Table II presents a list of the scale factors of both wing loading and dynamic similarity. Again, the density and gravity ratios are equal to 1.0.

TABLE II. - SCALE FACTORS USED FOR WING LOADING

Quantity	Ratio	Wing-loading result	Dynamic-similarity result
Wing loading	$R_{WL}$	1.0	$R_d$
Diameter	$R_d$	$R_d$	$R_d$
Area	$R_S$	$R_d^2$	$R_d^2$
Volume	$R_V$	$R_d^3$	$R_d^3$
Gravity	$R_g$	1.0	1.0
Air density	$R_\rho$	1.0	1.0
Structural density	$R_{\rho_s}$	$R_d^{-1}$	1.0
Distance	$R_x$	1.0	$R_d$
Velocity	$R_v$	1.0	$R_d^{1/2}$

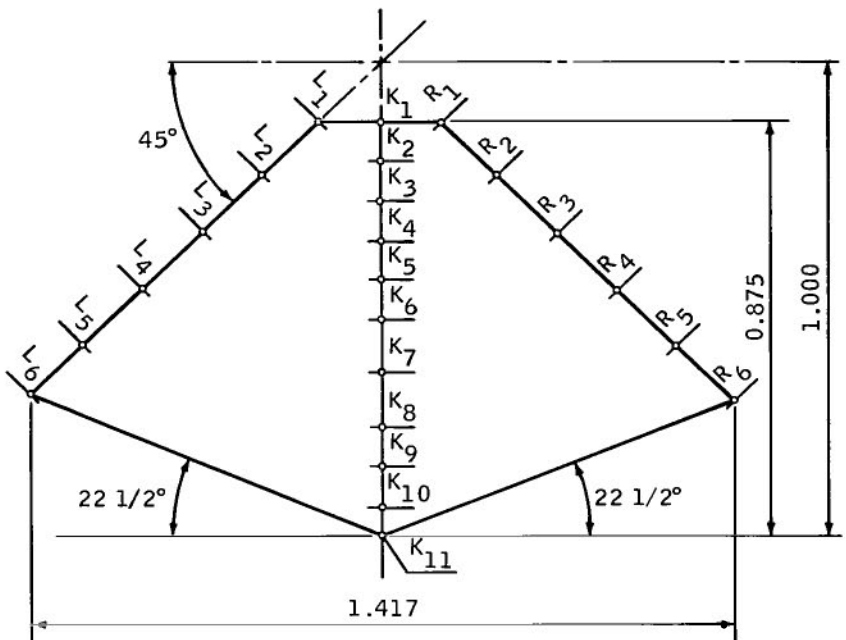
TABLE II. - SCALE FACTORS USED FOR WING LOADING - Concluded

Quantity	Ratio	Wing-loading result	Dynamic-similarity result
Acceleration	$R_v$	1.0	1.0
Time	$R_t$	1.0	$R_d^{1/2}$
Mass	$R_m$	$R_d^2$	$R_d^3$
Mass flow	$R_{\dot{m}}$	$R_d^2$	$R_d^{5/2}$
Weight	$R_W$	$R_d^2$	$R_d^3$
Drag coefficient	$R_{C_D}$	1.0	1.0
Lift coefficient	$R_{C_L}$	1.0	1.0
Flight-path angle	$R_\gamma$	1.0	1.0
Angular velocity	$R_\omega$	1.0	$R_d^{-1/2}$

## PARAWINGS AND TESTING COMPONENTS

The opening characteristics tests were performed in the Vehicle Assembly Building (VAB) at Kennedy Space Center, Florida. This building allowed constant indoor atmospheric conditions for the many required repeatable deployments. In addition, the building offered an unobstructed height of approximately 465 feet for the free-fall drops.

Three scaled, all-flexible parawings were tested: a small-scale model having a keel length of 8 feet, an intermediate-scale model having a keel length of 18 feet, and a full-scale model having a keel length of 24 feet. For simplicity, the keel lengths were chosen as the reference base length for all linear dimensions, including linear displacements involved in the solutions of velocities and accelerations for all parawings. Figure 1 presents the basic planform which was used in the construction of each parawing.



All dimensions referenced to keel length

Line	Line length	Distance from leading edge
R <sub>1</sub> and L <sub>1</sub>	1.333	0.177
R <sub>2</sub> and L <sub>2</sub>	1.281	.333
R <sub>3</sub> and L <sub>3</sub>	1.237	.500
R <sub>4</sub> and L <sub>4</sub>	1.167	.667
R <sub>5</sub> and L <sub>5</sub>	1.119	.833
R <sub>6</sub> and L <sub>6</sub>	1.001	1.000
K <sub>1</sub>	1.292	.125
K <sub>2</sub>	1.315	.208
K <sub>3</sub>	1.325	.292
K <sub>4</sub>	1.304	.375
K <sub>5</sub>	1.279	.458
K <sub>6</sub>	1.271	.542
K <sub>7</sub>	1.271	.646
K <sub>8</sub>	1.271	.750
K <sub>9</sub>	1.256	.833
K <sub>10</sub>	1.180	.917
K <sub>11</sub>	1.094	1.000

Figure 1. - Parawing canopy planform.

Components of the parawing-payload systems consisted of the canopy, the suspension lines, a riser with a quick-release snap ring, the load cell, and the lead sphere. Test components included the ceiling hoist line, a 24-V dc battery, an automatic release mechanism, a canopy packing sleeve, a free-fall control line, and the time-load recording apparatus. Figure 2 presents a schematic of all components involved.

### Parawing

Each parawing canopy was constructed of 2 oz/yd<sup>2</sup> low-porosity (3.5 ft<sup>3</sup>/ft<sup>2</sup>/min at 0.5 in. water) rip-stop nylon cloth cut identically in shape but scaled differently in overall dimension by definite ratios. Dimensions of the parawings, including suspension line lengths, are presented in figure 1. No attempt was made to scale the material properties since any effects caused by improper scaling in this area were considered negligible.

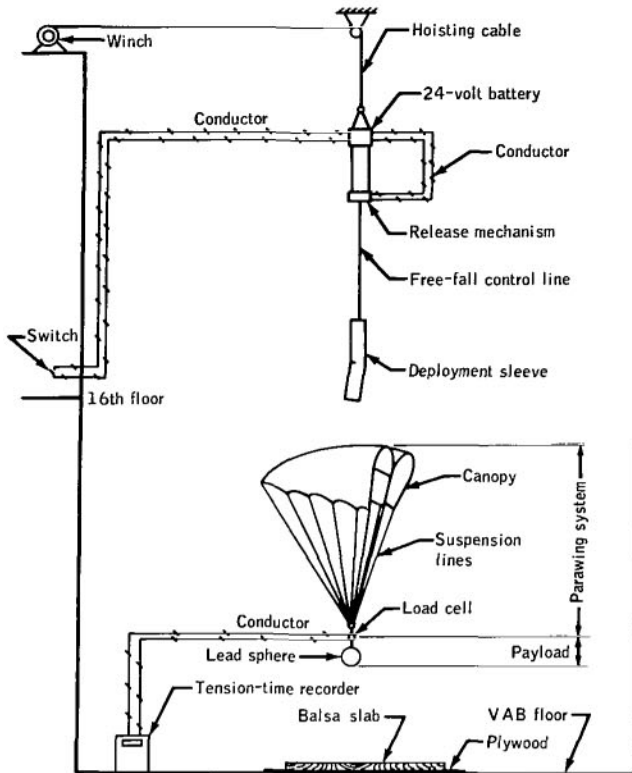


Figure 2. - General parawing payload with testing equipment.

#### Load-Measuring System

The load cells for each system were torus-shaped strain gages. A data hardline was connected to the load cell at one end and a multichannel strip chart at the other. With this arrangement, an accurate riser tension time history is recorded for each of the parawing drops. No noticeable effect on the tension time histories was caused by cable dynamics.

#### Payload

The payloads shown by figure 2 include the total weights beginning at the center of the load cell through all components down to and including the lead sphere. A breakdown of component weights for the total system of the three parawings is given in table III. Since the canopy weights do not scale properly, the weights of the lead spheres were adjusted to make the total weights correct. Dimensions of the lead spheres of all three parawings were scaled one to the other to obtain corresponding aerodynamic drag even though the drag was considered negligible in the calculations.

TABLE III. - SYSTEM WEIGHTS AND DIMENSIONS

	Parawing keel lengths, ft			
	8.0	18.0	24.0	8.0 (WL)
Canopy weight, lb	1.74	7.50	12.50	1.74
Load-cell weight, lb	.50	.56	.62	.50
Payload weight, lb	5.32	77.96	190.80	20.42
Total weight, lb	7.56	86.02	203.92	22.66
Scaled to 8 ft	7.56	7.55	7.55	
Scaled to 18 ft	86.11	86.02	86.77	
Scaled to 24 ft	204.12	202.15	203.92	203.94
24 ft, scaled to 8 ft (WL)			22.66	22.66

#### Canopy -Packing Sleeves

Canopy-packing sleeves (deployment sleeves) were made of cotton cloth cut in a rectangular pattern and sewn in a cylindrical shape. After folding, the parawings were inserted in the sleeves ready for deployment. Once the parawings were packed, a lightweight break cord was tied between the sleeve and the canopy to insure that the canopy did not deploy prematurely. Also, the break cord provides a positive indication of deployment on the trace of tension time plots.

#### Automatic Release Mechanism

The parawing automatic release mechanism consisted of a hand-cocked, spring-loaded cutting blade, which is released by a solenoid. Upon command, the cutting blade severs a light cord lashing the packed canopy to the cutter, which thereby causes the parawing-payload system to drop.

#### DEPLOYMENT TEST

In general, the sequence of events involved in the preparation of a drop are folding and inserting the canopy into the sleeve, tightly lashing both canopy and sleeve

to the release mechanism, and lifting the entire system to predeployment elevation. The parawing for each drop was folded accordian style with the width of each fold scaled properly. The fold was begun at the trailing edge of the parawing, and an attempt was made to prevent any irregularities in folding from drop to drop. Figure 3 shows the folding of a parawing. Figure 4 shows the folded parawing being inserted into the sleeve. Figure 5 shows a parawing system positioned for deployment.



Figure 3. - Parawing folding technique.

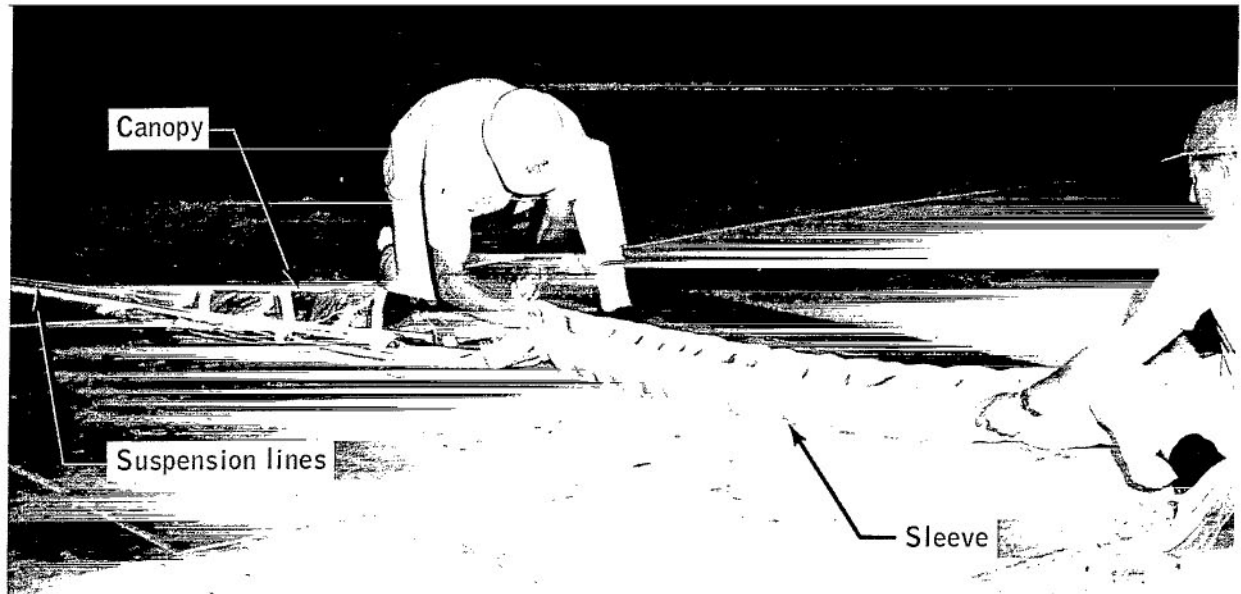


Figure 4. - Parawing packing technique.

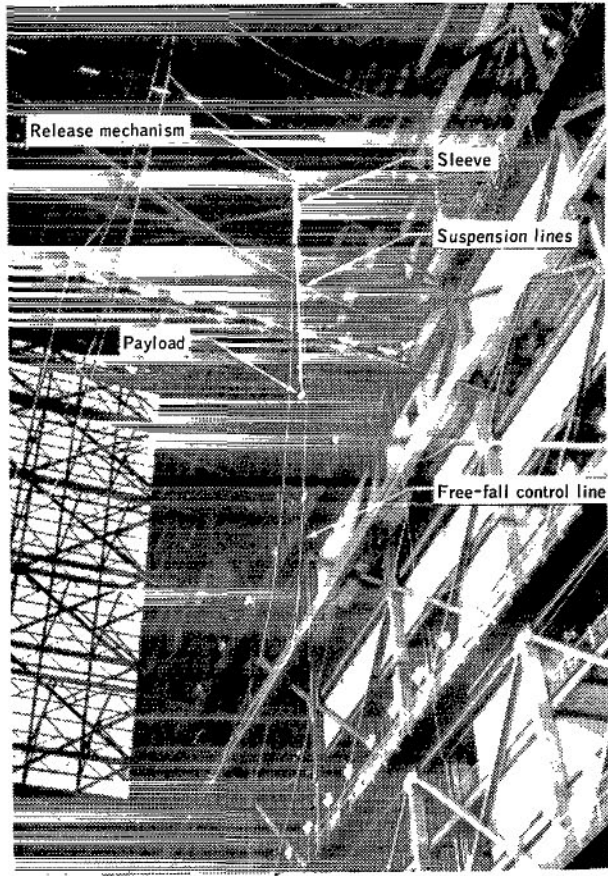


Figure 5.- Parawing positioned for deployment.

The packed parawing and the payload, when released, are allowed to free fall a definite distance to obtain a particular velocity. This velocity is termed the initial deployment velocity throughout the tests. The free-fall distance is controlled by a draped line attached between the release mechanism and the top of the sleeve. Upon release, the system falls to the end of the draped line and causes extraction of the canopy and thus commencement of opening. The sequence of events involved in deployment are release, free fall, extraction, commencement of opening, full opening, and transition to glide. A complete pictorial history of the events is shown in figure 6. Figure 6 shows that peak tension occurs just as the canopy reaches full open ( $t = 3.02$  sec) and, immediately following, pitches over into the glide angle ( $t = 3.52$  sec).

A series of drops, each with three different free-fall control lines, was performed on the three parawings. The control lines gave initial opening velocities for the parawings as follows: (1) small-scale model, 46.3, 51.8, and 56.7 fps; (2) intermediate-scale model, 69.5, 77.7, and 85.1 fps; and (3) full-scale model, 80.2 and 89.7 fps. One series of drops was made on the small-scale model at a deployment velocity of 80.2 fps, which was used for scaling by wing loading.

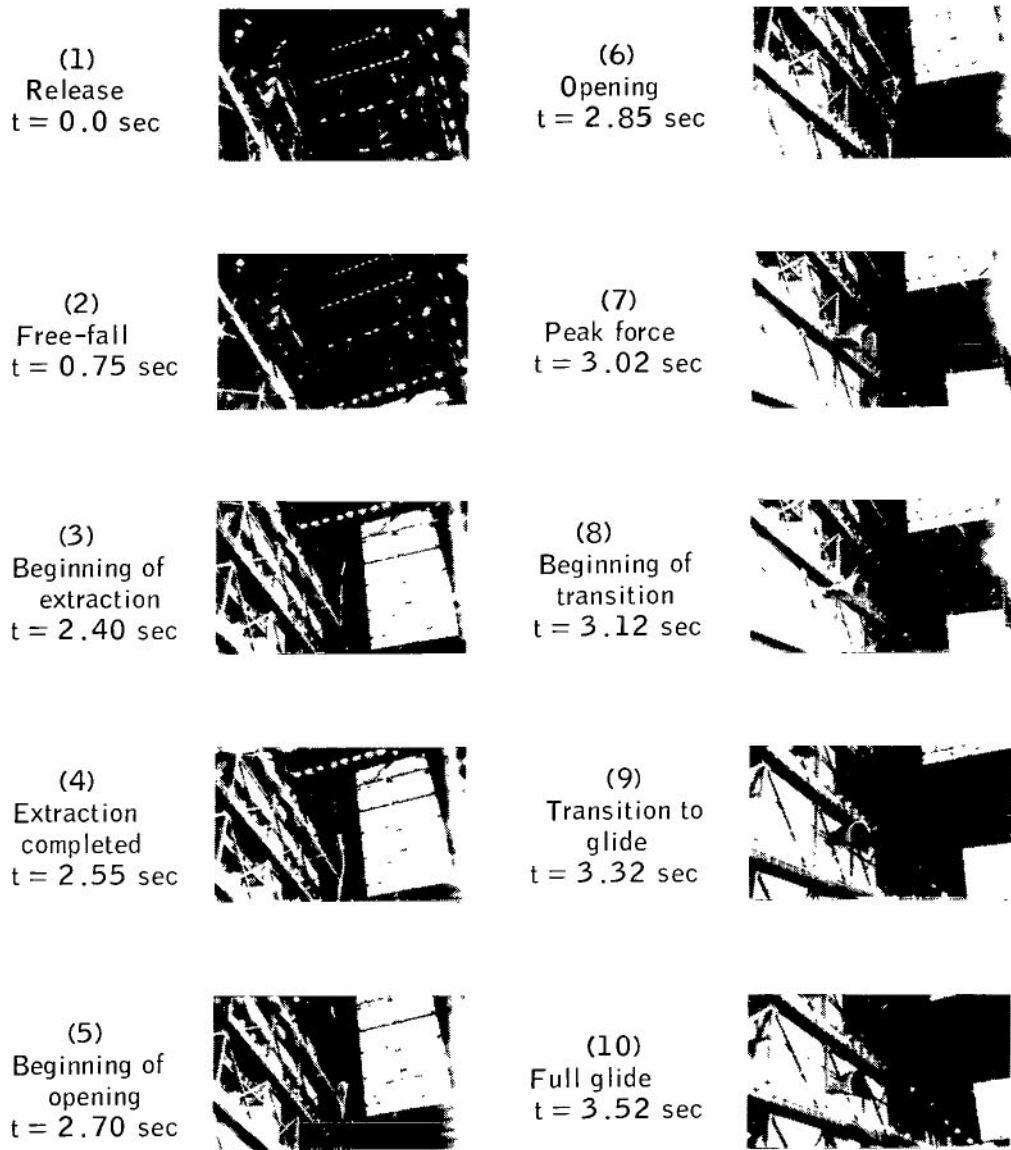


Figure 6.- Deployment sequence of intermediate model parawing.

## DATA REDUCTION

Acceleration, velocity, and displacement time histories were computed by considering the payload equation of motion in vertical descent

$$m_{P.L.} \dot{v} = T + D - W_{P.L.} \quad (32)$$

It is assumed that the payload drag is negligible and that the riser line tension acts along the vertical. The riser line will be parallel to the gravity vector until sufficient lift in the parachute has caused a measurable pitch angle. Analysis of motion-picture data indicates that this occurs just after peak tension at which time the data reduction equations no longer hold. Solving equation (32) with  $\dot{v}(0) = 0$  for the acceleration yields

$$\dot{v} = \frac{T}{m} - g \quad (33)$$

Integration yields the velocity

$$v = \int \left( \frac{T}{m} - g \right) dt \quad (34)$$

Integrating again yields displacement

$$x = \int v dt = \int \int \left( \frac{T}{m} - g \right) dt dt \quad (35)$$

Since the same weight-per-unit area cloth was used in the construction of the parawings, the canopy properties did not scale properly. To compensate partially for this, as noted previously, the payload weight was adjusted to make the total system weight scale correctly. Compensating in this manner required a correction technique which was derived and validated in reference 2. Table IV presents the correction factors used in the data reduction.

TABLE IV. - TENSION CORRECTION FACTOR<sup>a</sup>

$$\left[ T_f = T_m R_d^{-3} CF \right]$$

Model, ft	Full scale, ft	Correction factor
8	18	1.21
8	24	1.26
18	24	1.04
8 (WL)	24 (WL)	1.03

<sup>a</sup>Reference 2.

## RESULTS

### Repeatability

Although an effort was made to minimize the scatter of data by the described methods of deployments, the spread is spontaneous and appears to be characteristic of flexible parachute deployment. Repeatability spread is unavoidably present in each series of deployment tests and is verified by the tension time plots. The differences are resultants of many very small elementary differences, including the effects of the following variables (ref. 3):

1. Variable friction of sleeve to canopy because of packing
2. Twisting and tanglement of suspension lines
3. Aerodynamic turbulence in the wake of the payload and suspension lines

Predicting results on the full scale from observations on the model requires an adequate number of drops to establish the most probable representative value. The degree of accuracy relative to the representative value is a function of the number of drops made. Obtaining a complete statistical description (requiring many drops) was prohibitive and considered secondary to scaling verification. Based upon the degree of scatter, only four or five drops were made to establish the value for all cases.

### Small-Scale Model Deployment Characteristics

The actual tension time histories of the small-scale parawing for the low, medium, and high velocities are presented in figure 7. The plots shown in figure 7(a) are the combined histories of the 8-foot parawing with a deployment velocity of 46.3 fps. The deployment sequence is as follows: release at 0 second, free fall until approximately 1.5 seconds, extraction at the small peak followed by a larger peak at maximum tension, and the beginning of transition to glide. The plot in figure 7(b) is similar, but the deployment velocity is 51.8 fps. Events in the tension time history occur a little later than in figure 7(a), and maximum tension has some increases. The deployment velocity of figure 7(c) is 56.7 fps, and the timing and tension are greater than in the two previous cases.

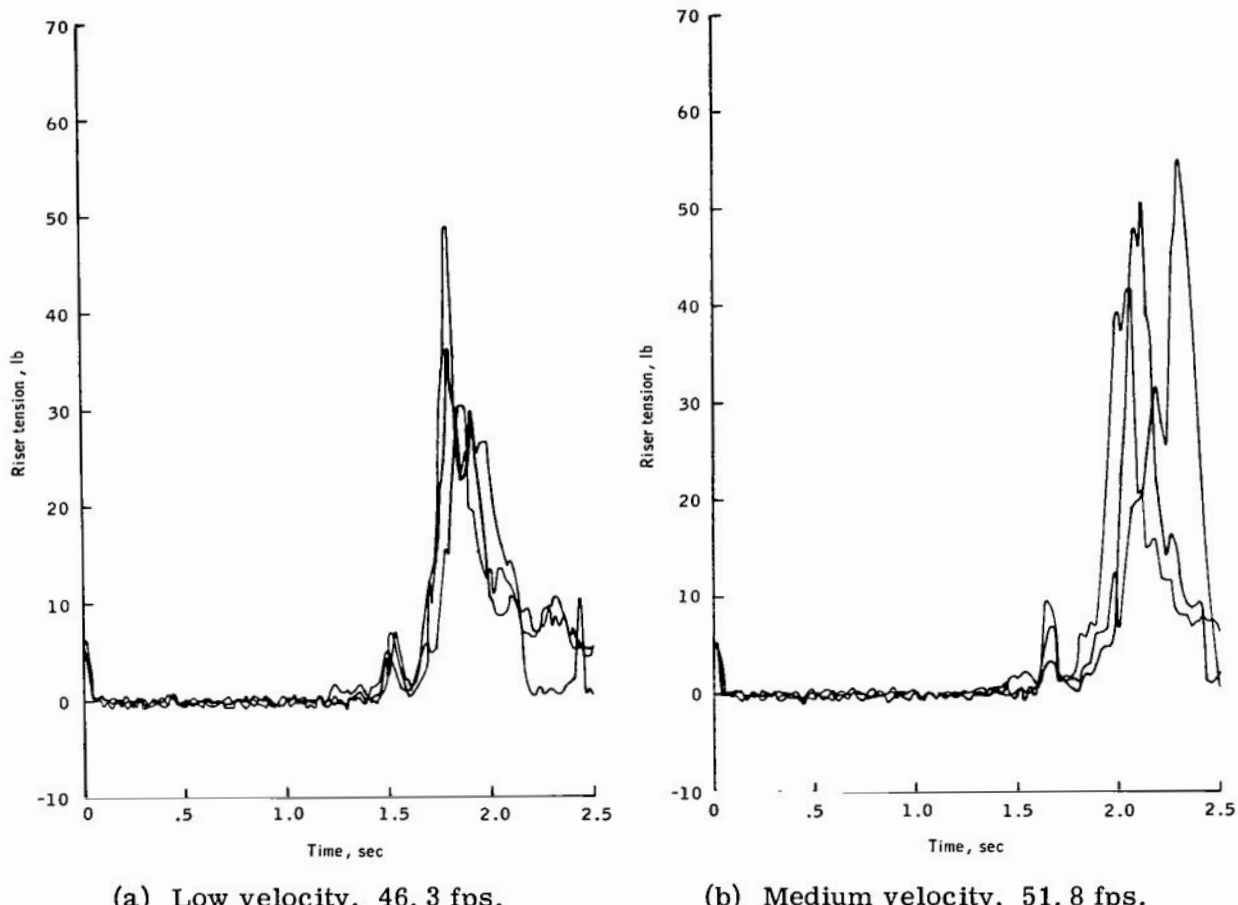
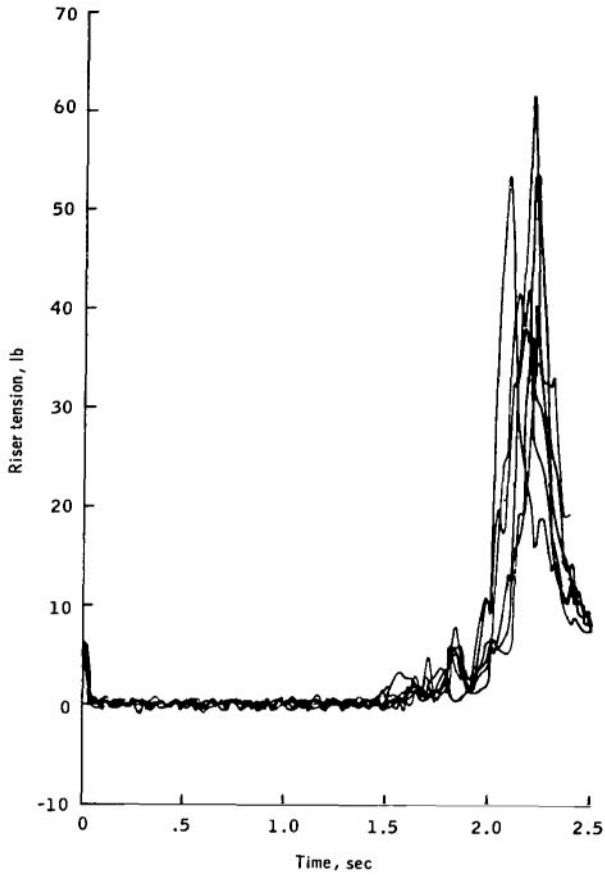


Figure 7. - Small-scale model deployment characteristics.

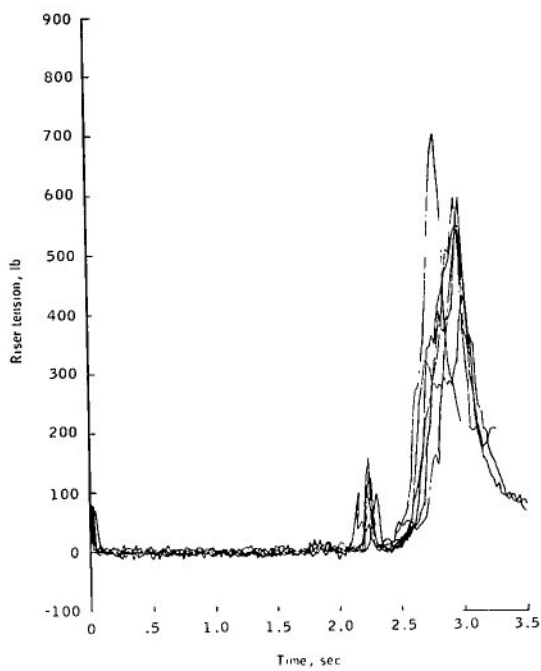


(c) High velocity, 56.7 fps.

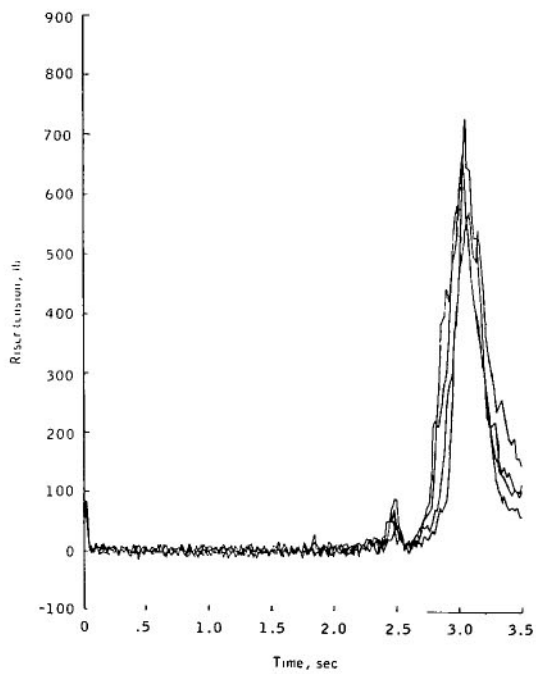
Figure 7. - Concluded.

#### Intermediate-Scale Model Deployment Characteristics

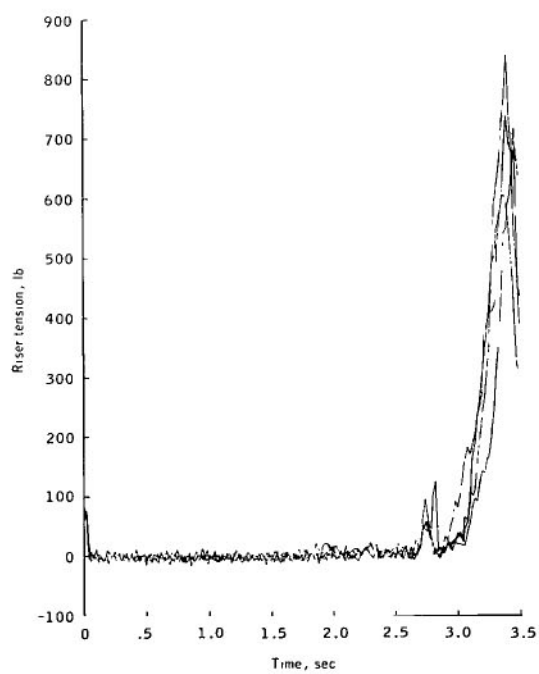
The tension time histories of the intermediate-model parawing are presented in figure 8. In figure 8(a), the deployment velocity was 69.5 fps. In these low-velocity cases, extraction occurred at approximately 2.25 seconds and peak tension at approximately 3.0 seconds. The deployment velocity in figure 8(b) was 77.7 fps; and, as noted for the small-scale parawing traces, as the velocity increases, events occur later and the tensions are higher. Figure 8(c) represents the high-velocity cases with a velocity of 85.1 fps.



(a) Low velocity, 69.5 fps.



(b) Medium velocity, 77.7 fps.

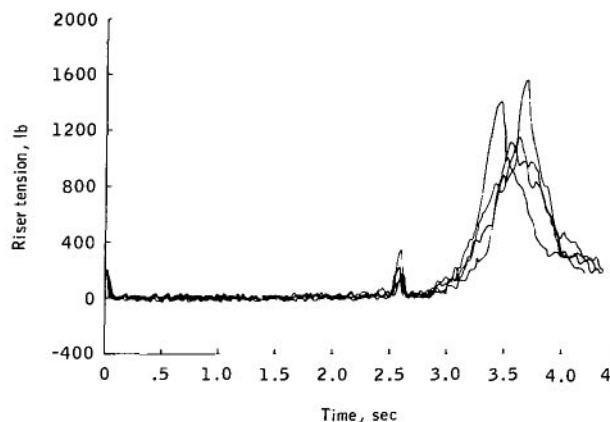


(c) High velocity, 85.1 fps.

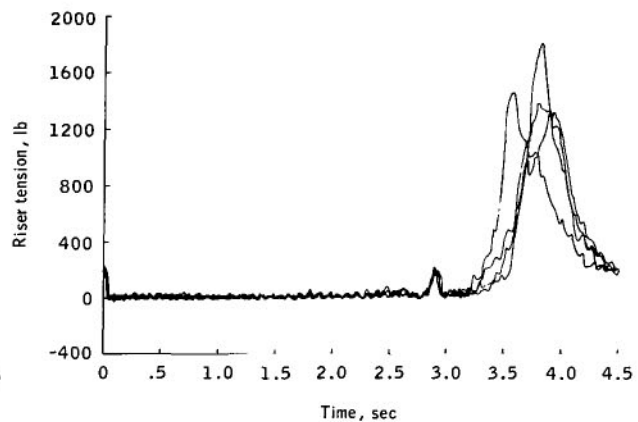
Figure 8. - Intermediate-scale model deployment characteristics.

## Full-Scale Model Deployment Characteristics

The low- and medium-velocity cases for the 24-foot parawing are presented in figure 9 in a manner identical to figures 7 and 8. Figure 9(a) represents the low-velocity cases with a deployment velocity of 80.2 fps. The deployment velocity in figure 9(b) was 89.7 fps, which corresponds to the medium-velocity cases of the 8- and 18-foot parawings. In general, the traces all have the same shape, and the degree of repeatability in any case is the same. In each series of deployments, the small rise in tension that occurs at extraction was caused by the break cord attached between the parawing canopy and the sleeve. No deployments were made with the full-scale parawing at the high-velocity case of 98.2 fps because of safety precautions and the restrictive nature of the test facilities. Even without this series of deployments, the test objectives were satisfied adequately.



(a) Low velocity, 80.2 fps.



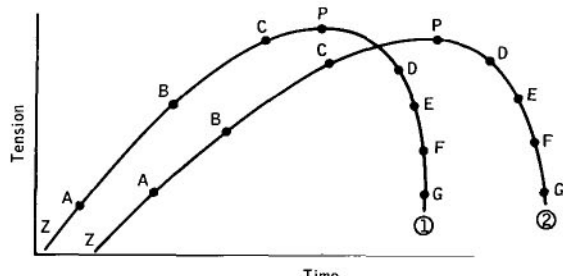
(b) Medium velocity, 89.7 fps.

Figure 9.- Full-scale deployment characteristics.

### Averaging Technique

Since the time of occurrence of an event is equally important in scaling with the physical parameter (in this case, peak tension), the averaging was done to reflect both.

By taking  $n$  number of tension time traces, as shown in the schematic, the peak tension is averaged as follows:



$$T_{\text{peak, avg}} = \frac{T_{1P} + T_{2P} + \dots + T_{nP}}{n}$$

Because of equal interest in when the average peak tension occurs, the time to peak is averaged by

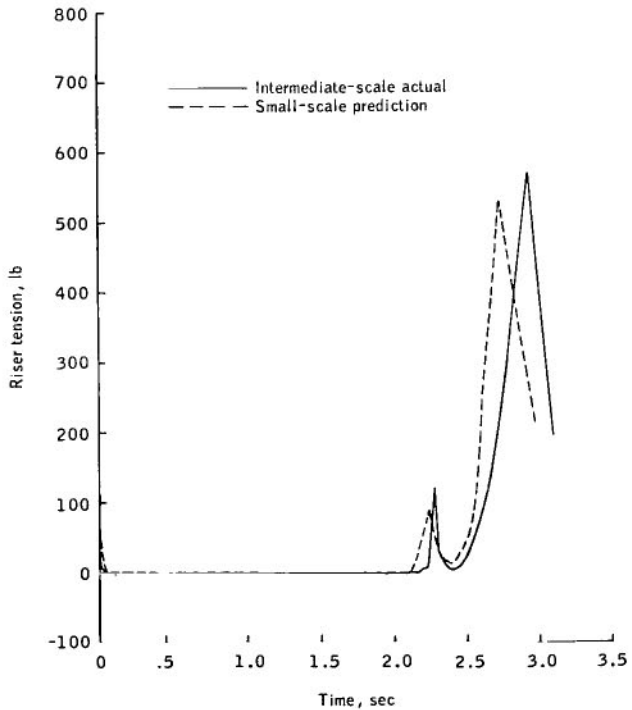
$$t_{\text{peak, avg}} = \frac{t_{1P} + t_{2P} + \dots + t_{nP}}{n} \quad (36)$$

To develop a representative curve, more than the peak tension point is needed. Thus, for each curve, the last point of zero tension (Z) was used; and, between this point and peak tension, points of similarity (points A to C) were selected for averaging. The tension at these points and the times of occurrence were averaged in the manner previously described. In a similar manner, the negative slope of each trace (points D to G) was averaged, which led to the representative curve.

Similarly, the averaging for the acceleration, velocity, and distance time histories was done, but the time of occurrence was fixed by the times used with the tension time histories.

### Dynamic-Similarity Results

To make comparisons using the various sets of data, averages of the data were used. Initially, the averages of the small-scale model were used to predict those of the intermediate-scale model. The averages were predicted in accordance with the derived scale factors by multiplying the tension by the inverse of the force ratio (11.39) and the force correction factor (1.21) and multiplying the time by the inverse of the time ratio (1.5). The comparisons of the small-scale predictions and the actual intermediate-scale tension time histories are presented in figure 10. The small-scale prediction is the dashed line and the intermediate-scale average is the solid line. The extraction peaks always match well, and the maximum tensions are well within the repeatability of the data. The acceleration time histories were computed and averaged as before. The small-scale model data then were used to predict the intermediate-scale model data according to the scaling ratios and are presented for comparison in figure 11. The results indicate that model acceleration data can be used to predict larger-scale



(a) Low velocity, 69.5 fps.

Figure 10. - Comparison of small-scale predicted and intermediate-scale average tension time histories.

data. After peak negative acceleration, the data reduction equations do not account for the observed lift.

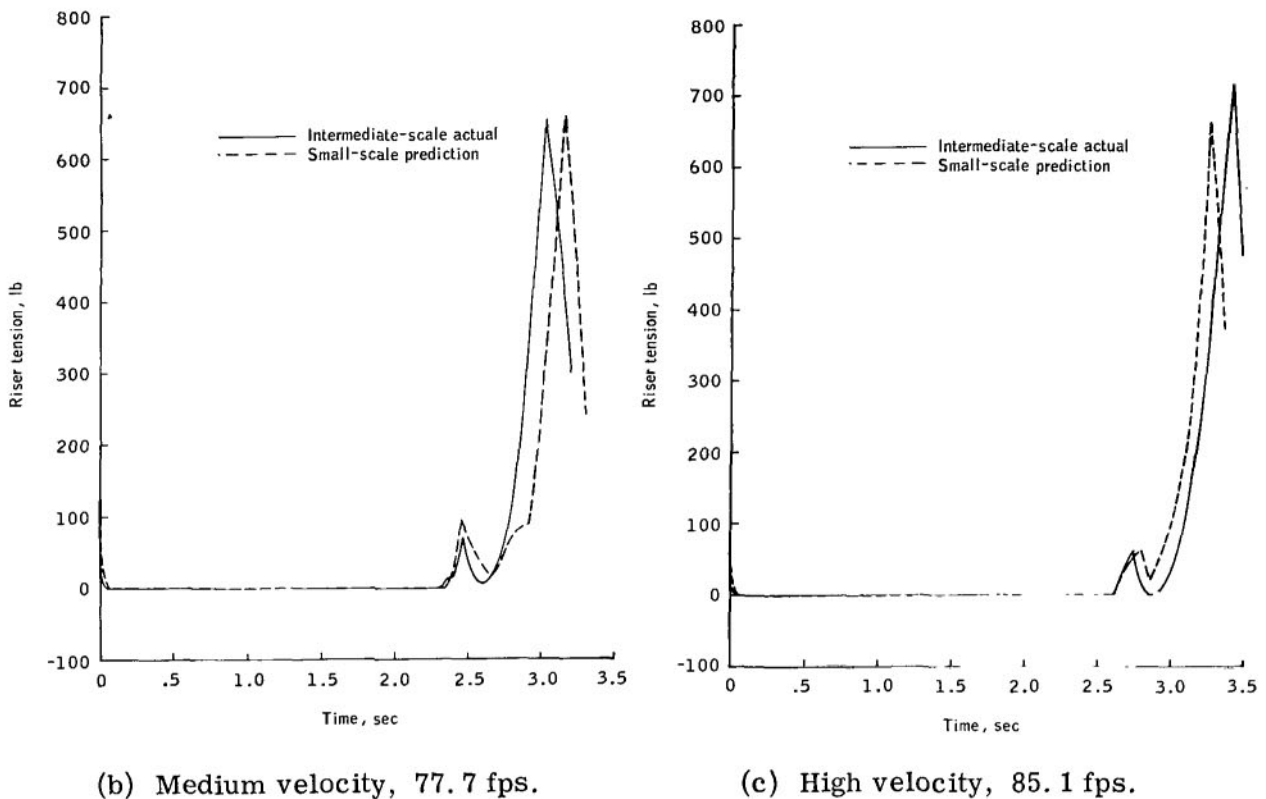
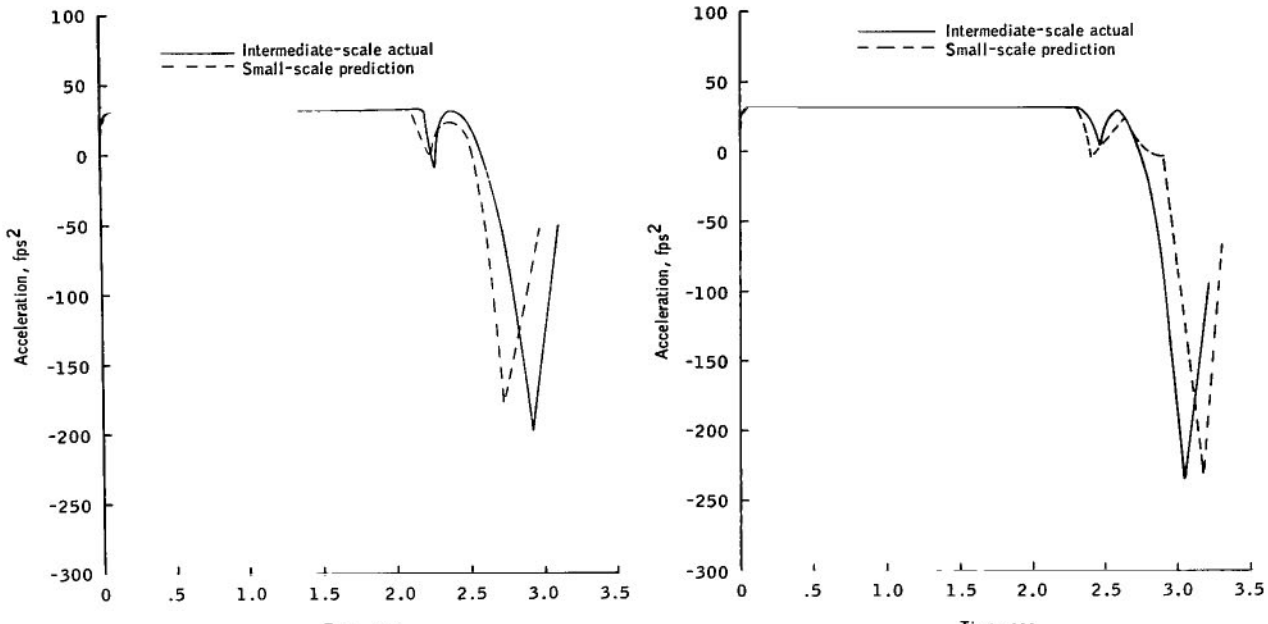


Figure 10. - Concluded.

In much the same manner, figures 12 and 13 were constructed to compare the velocity and distance time histories. All differences become less pronounced as the integration routine averages the difference. The small-scale model results predict the intermediate-scale data very accurately.

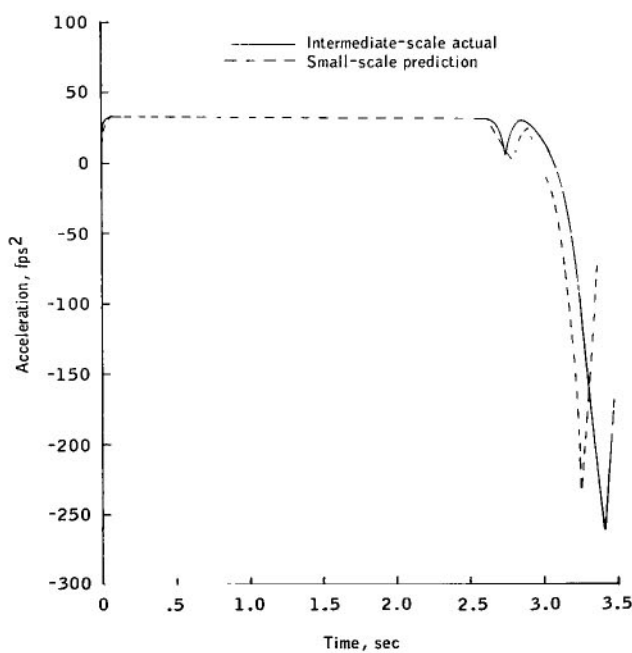
Next, the small- and intermediate-scale averages were scaled by the proper scaling ratios to predict the average results of the full-scale tensions, accelerations, velocities, and distances. The comparison of the predicted and actual tension time histories is presented in figure 14. Full-scale data are represented by the solid line, intermediate-scale data are represented by the broken line, and small-scale model data are represented by the dashed line. Again, in both cases, the extraction peaks match very well, and the peak tensions fall within the repeatability of the data, which indicates that full-scale data can be predicted by models.

Figure 15 presents a comparison of predicted and actual acceleration time histories. Figure 16 presents velocity time histories and figure 17 presents distance time histories. The results confirm that full-scale opening characteristics can be predicted from model data with ratios ranging from 1:1.33 to 1:3.



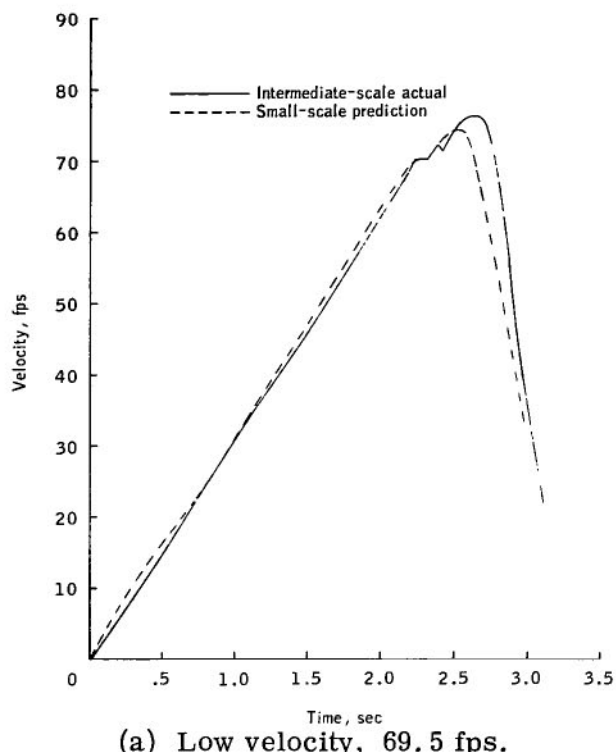
(a) Low velocity, 69.5 fps.

(b) Medium velocity, 77.7 fps.

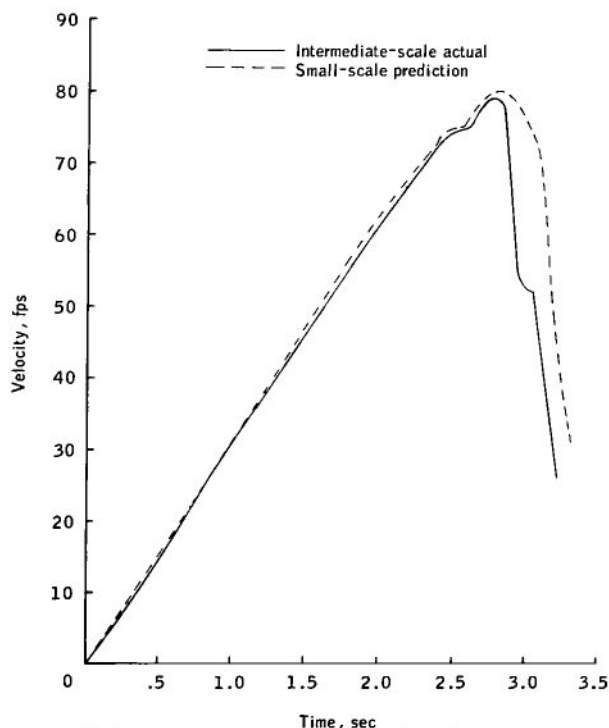


(c) High velocity, 85.1 fps.

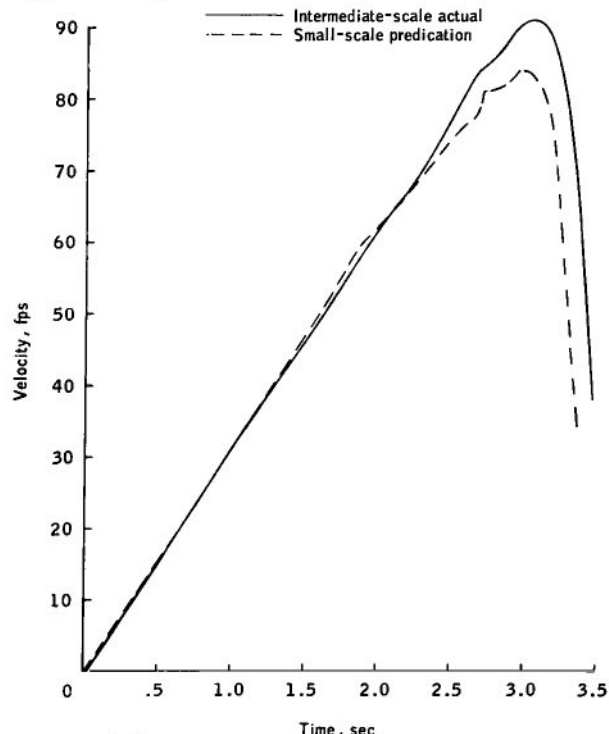
Figure 11. - Comparison of small-scale predicted and intermediate-scale average acceleration time histories.



(a) Low velocity, 69.5 fps.

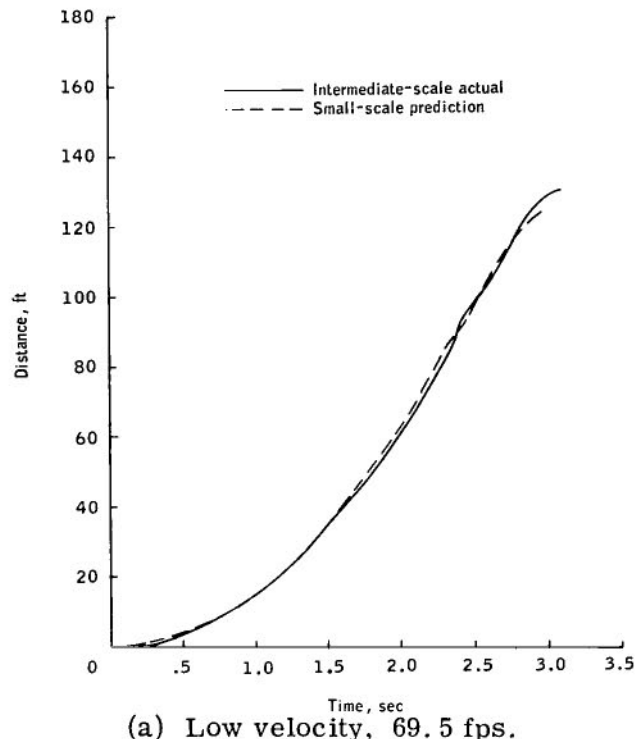


(b) Medium velocity, 77.7 fps.

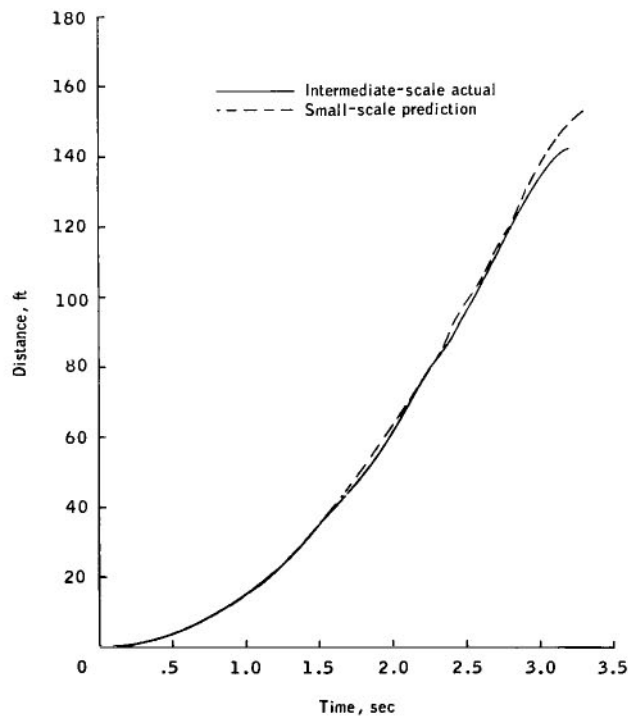


(c) High velocity, 85.1 fps.

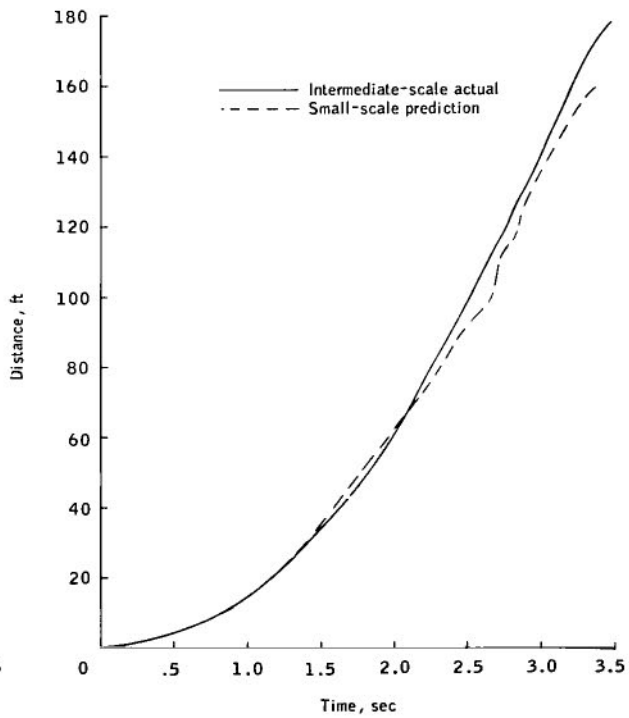
Figure 12. - Comparison of small-scale predicted and intermediate-scale average velocity time histories.



(a) Low velocity, 69.5 fps.



(b) Medium velocity, 77.7 fps.



(c) High velocity, 85.1 fps.

Figure 13. - Comparison of small-scale predicted and intermediate-scale average distance time histories.

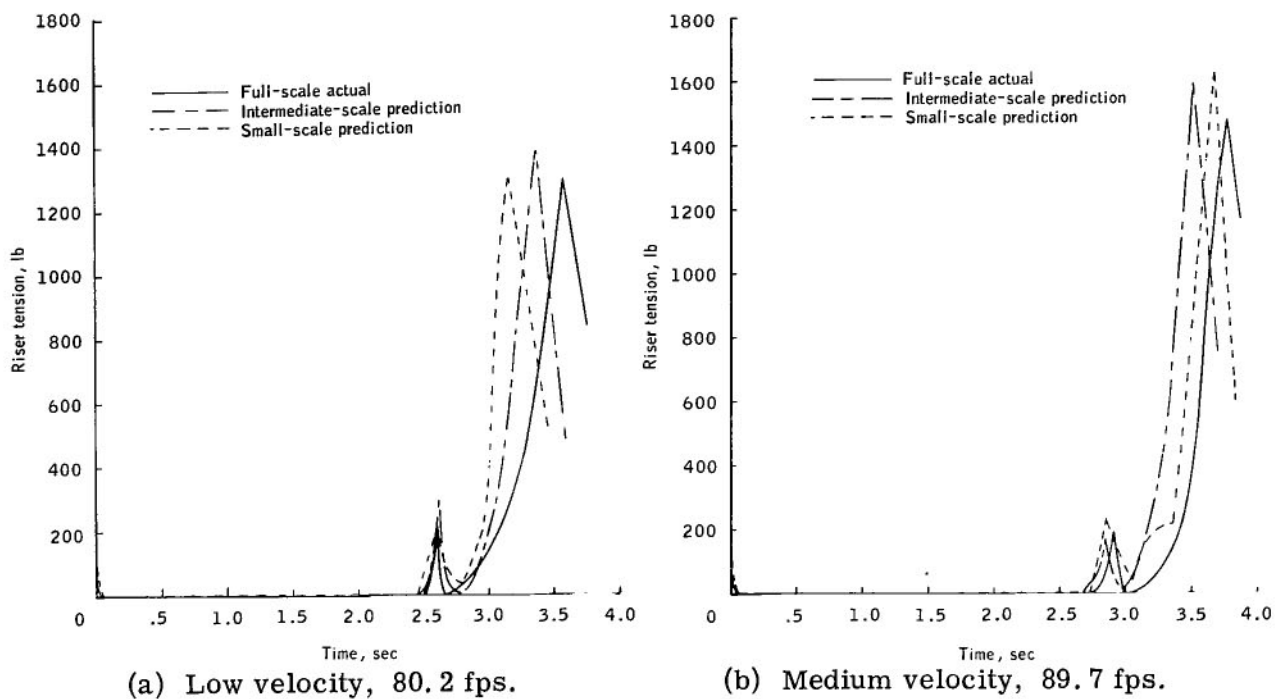


Figure 14.- Comparison of small- and intermediate-scale predicted and full-scale average tension time histories.

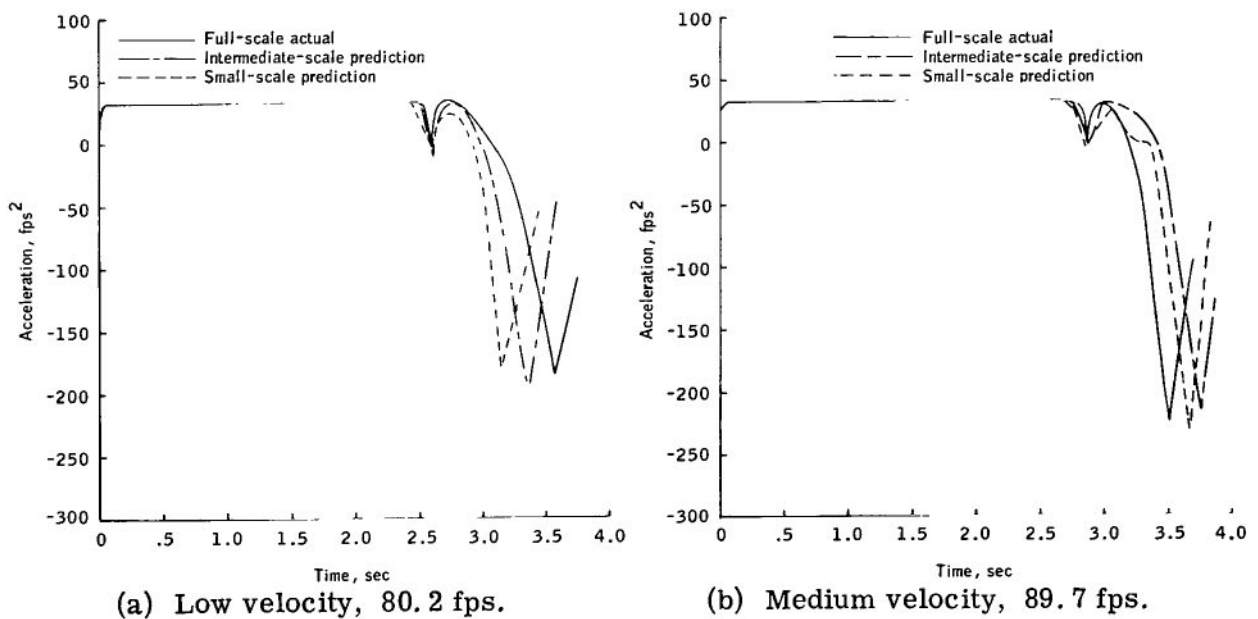
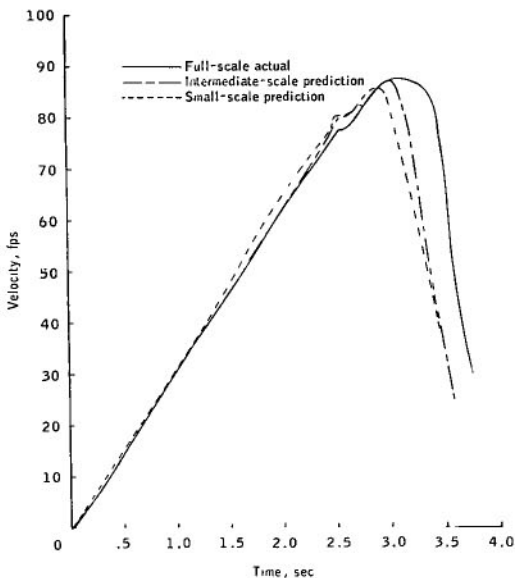
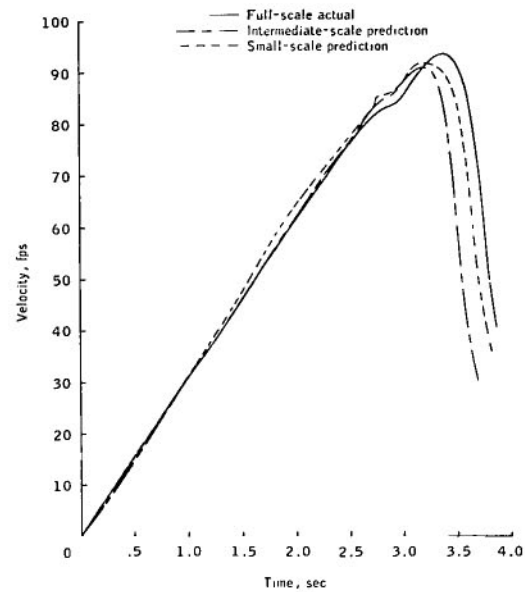


Figure 15.- Comparison of small- and intermediate-scale predicted and full-scale average acceleration time histories.

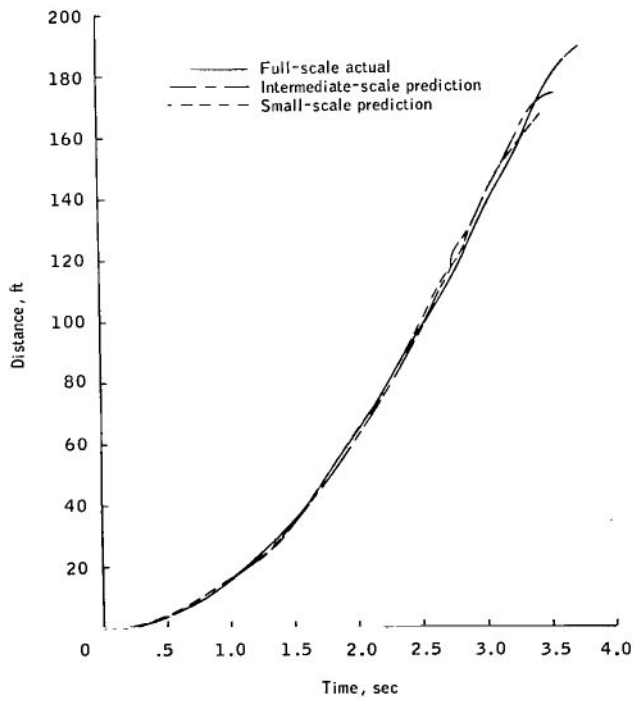


(a) Low velocity, 80.2 fps.

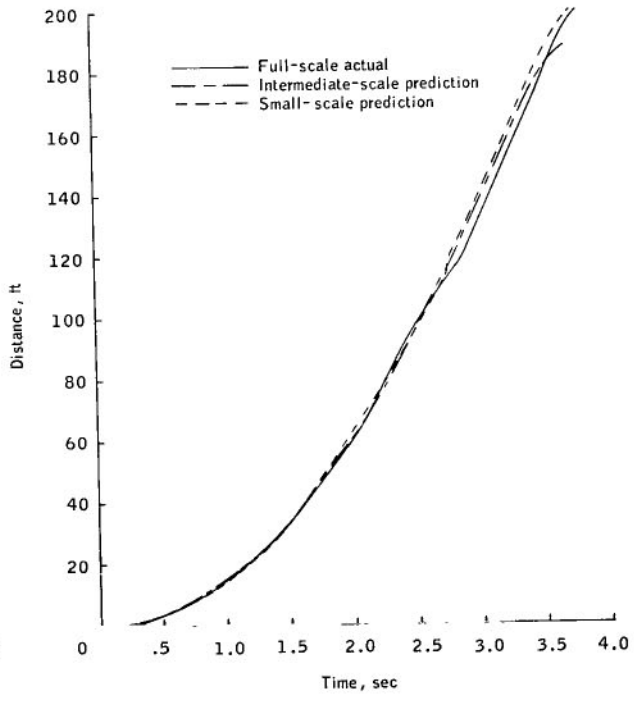


(b) Medium velocity, 89.7 fps.

Figure 16. - Comparison of small- and intermediate-scale predicted and full-scale average velocity time histories.



(a) Low velocity, 80.2 fps.



(b) Medium velocity, 89.7 fps.

Figure 17. - Comparison of small- and intermediate-scale predicted and full-scale average distance time histories.

### Wing-Loading Results

To ascertain the validity of scaling by matching the wing loading of the parawings ( $R_{WL} = 1.0$ ), a series of low-velocity deployments (80.2 fps) was made with the small-scale parawing in an attempt to predict the full-scale, low-velocity data. Figure 18 presents the small-scale deployment characteristics based upon the guidelines established by the wing-loading scale factors. These data then were averaged as described previously. The model tensions were multiplied by the inverse of the wing-loading force ratio (9) and the tension correction factor (1.03), while the time remained the same ( $R_{tWL} = 1.0$ ), to give the wing-loading prediction of the full-scale characteristics. A comparison of this prediction and the actual averaged (from fig. 14(a)) tension time histories is presented in figure 19. From figure 19, it can be seen that the model data not only predict an earlier opening time but also overpredict the peak tension.

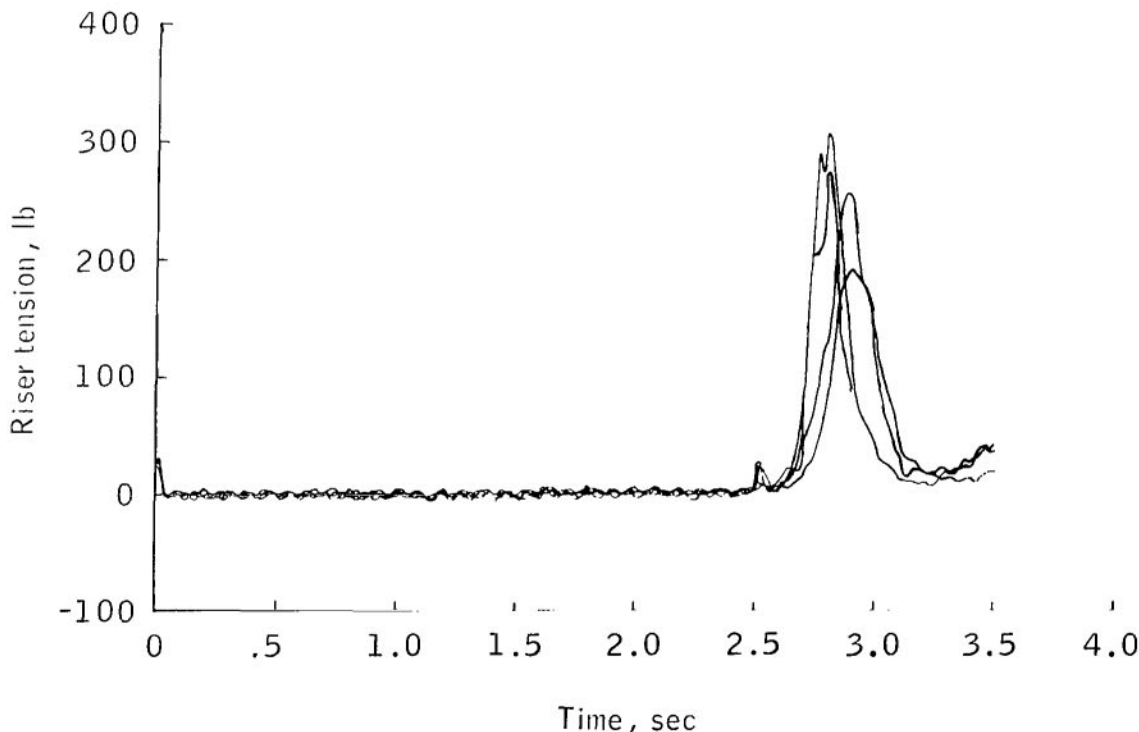


Figure 18. - Small-scale deployment characteristics (based on wing loading); velocity = 80.2 fps.

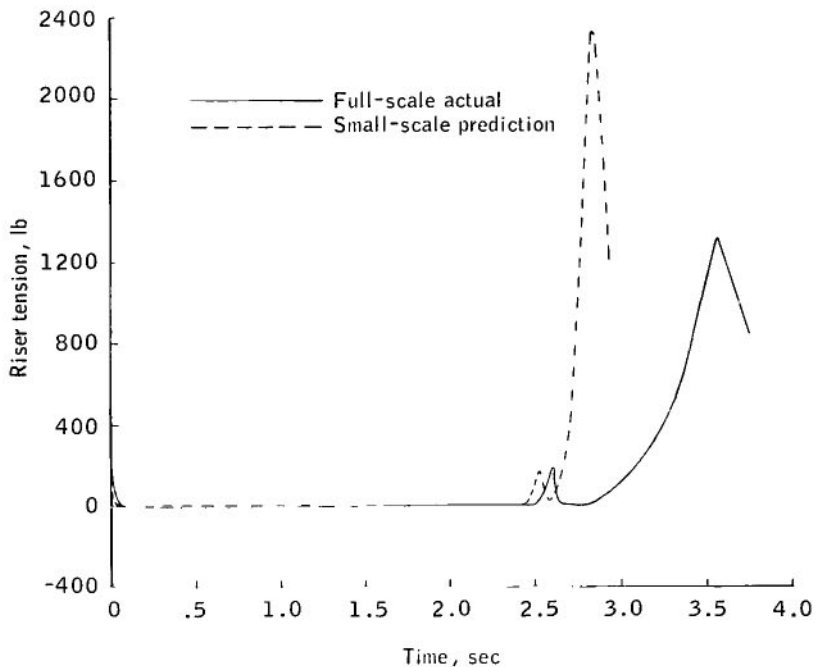


Figure 19. - Comparison of predicted and average tension time histories (based on wing loading); velocity = 80.2 fps.

#### CONCLUDING REMARKS

From the results presented, the following conclusions are reached.

1. The principle of dynamic similarity provides a valid scaling method.
2. Dynamic similarity was used successfully to predict opening characteristics of parawings with diameter ratios as great as 1:3 within the boundary conditions of the test program.
3. Forcing the weight-per-unit canopy area of the model and full-scale parawing to be equal is not a satisfactory method of scaling.

Manned Spacecraft Center  
 National Aeronautics and Space Administration  
 Houston, Texas, December 4, 1968  
 961-21-30-09-72

## REFERENCES

1. Barton, Richard L.: Scale Factors for Parachute Opening. NASA TN D-4123, 1967.
2. Eichblatt, David L.; Moore, Robert H.; and Barton, Richard L.: Experimental Verification of Scale Factors for Parawing Opening Characteristics. NASA TN D-4665, 1968.
3. Gray, J. Harvey: Attenuation of Deployment and Opening Forces of Certain Aerodynamic Decelerators. Paper presented at Symposium on Parachute Technology and Evaluation (Edwards Air Force Base, Calif.), Sept. 1964.

NATIONAL AERONAUTICS AND SPACE ADMINISTRATION

WASHINGTON, D. C. 20546

OFFICIAL BUSINESS

POSTAGE AND FEES PAID  
NATIONAL AERONAUTICS AND  
SPACE ADMINISTRATION

FIRST CLASS MAIL

POSTMASTER: If Undeliverable (Section 158  
Postal Manual) Do Not Return

*"The aeronautical and space activities of the United States shall be conducted so as to contribute . . . to the expansion of human knowledge of phenomena in the atmosphere and space. The Administration shall provide for the widest practicable and appropriate dissemination of information concerning its activities and the results thereof."*

— NATIONAL AERONAUTICS AND SPACE ACT OF 1958

## NASA SCIENTIFIC AND TECHNICAL PUBLICATIONS

**TECHNICAL REPORTS:** Scientific and technical information considered important, complete, and a lasting contribution to existing knowledge.

**TECHNICAL NOTES:** Information less broad in scope but nevertheless of importance as a contribution to existing knowledge.

**TECHNICAL MEMORANDUMS:** Information receiving limited distribution because of preliminary data, security classification, or other reasons.

**CONTRACTOR REPORTS:** Scientific and technical information generated under a NASA contract or grant and considered an important contribution to existing knowledge.

**TECHNICAL TRANSLATIONS:** Information published in a foreign language considered to merit NASA distribution in English.

**SPECIAL PUBLICATIONS:** Information derived from or of value to NASA activities. Publications include conference proceedings, monographs, data compilations, handbooks, sourcebooks, and special bibliographies.

**TECHNOLOGY UTILIZATION PUBLICATIONS:** Information on technology used by NASA that may be of particular interest in commercial and other non-aerospace applications. Publications include Tech Briefs, Technology Utilization Reports and Notes, and Technology Surveys.

*Details on the availability of these publications may be obtained from:*

**SCIENTIFIC AND TECHNICAL INFORMATION DIVISION**

**NATIONAL AERONAUTICS AND SPACE ADMINISTRATION**

Washington, D.C. 20546